Kinetics of OH Radical Reaction with Anthracene and Anthracene-d_{10}

Rajeshwar Ananthula,* Takahiro Yamada, and Philip H. Taylor*

Environmental Engineering Group, University of Dayton Research Institute, 300 College Park, Dayton, Ohio 45469-0114

Received: August 3, 2005; In Final Form: January 18, 2006

Using a refined pulsed laser photolysis/pulsed laser-induced fluorescence (PLP/PLIF) technique, the kinetics of the reaction of a surrogate three-ring polynuclear aromatic hydrocarbons (PAH), anthracene (and its deuterated form), with hydroxyl (OH) radicals was investigated over the temperature range of 373 to 1200 K. This study represents the first examination of the OH kinetics for this class of reactions at elevated temperatures (>470 K). The results indicate a complex temperature dependence similar to that observed for simpler aromatic compounds, e.g., benzene. At low temperatures (373−498 K), the rate measurements exhibited Arrhenius behavior ($k = 1.82 \times 10^{-11}$ exp(542.35/T) in units of cm^3 molecule^{-1} s^{-1}), and the kinetic isotope effect (KIE) measurements were consistent with an OH-addition mechanism. The low-temperature results are extrapolated to atmospheric temperatures and compared with previous measurements. Rate measurements between 673 and 923 K exhibited a sharp decrease in the magnitude of the rate coefficients (a factor of 9). KIE measurements under these conditions were still consistent with an OH-addition mechanism. The following modified Arrhenius equation is the best fit to our anthracene measurements between 373 and 923 K (in units of cm^3 molecule^{-1} s^{-1}): k_1 (373−923 K) = 8.17×10^{14} $T^{-8.3}$ exp(−3171.71/T). For a limited temperature range between 1000 and 1200 K, the rate measurements exhibited an apparent positive temperature dependence with the following Arrhenius equation, the best fit to the data (in units of cm^3 molecule^{-1} s^{-1}): k_1 (999−1200 K) = 2.18×10^{-11} exp(−1734.11/T). KIE measurements above 999 K were slightly larger than unity but inclusive regarding the mechanism of the reaction. Theoretical calculations of the KIE indicate the mechanism of reaction at these elevated temperatures is dominated by OH addition with H abstraction being a minor contributor.

Introduction

The combustion of hydrocarbon fuels is a rapidly evolving area of macro-scale kinetic modeling.[1,2] OH radicals and small aromatic and multi-ring PAH compounds are among the key players in the fierce competition between pyrolysis processes leading to carbonaceous byproducts (fullerenes, single-wall carbon nanotubes)[3,4] and oxidation processes resulting in higher yields of oxidation products (highly efficient combustion engines). Depending on the desired outcome, a detailed knowledge of oxidation mechanisms initiated by molecular oxygen, O atoms, and OH radicals is of crucial importance for the determination of controlling parameters and the optimization of experimental conditions.

PAHs are believed to play a major role in the formation of soot and fine particulates in high-temperature combustion processes. A significant research effort on the chemistry of formation of PAHs has occurred in recent years.[5−8] Less research has been focused on the oxidation of PAH.[9] In particular, there is a lack of kinetic data on PAH + OH reactions at elevated temperatures. Benzene represents the only aromatic molecule for which an extended set of published OH rate measurements exist from room temperature up to postcombustion temperatures. The lack of PAH − OH reaction kinetics at elevated temperatures is the primary motivation for this research. The kinetic measurements presented herein are also relevant to the development of macroscopic models of complex atmospheric processes, such as those responsible for troposphere ozone and smog formation over urban areas.[10,11] These models place a high demand on accurate kinetic data for elementary reactions describing the OH radical-initiated atmospheric degradation of aromatic compounds.

Naphthalene was selected as the initial PAH surrogate to study. However, fluorescence at the same wavelength of the OH measurements (306 nm) attributed to substrate absorption of the probe laser radiation (282.2 nm) precluded accurate kinetic measurements. Thus, the focus of this study was changed to a three-ring surrogate PAH, anthracene, for which absorption cross-sections[12] at 282.2 nm were a factor of 10−20 times lower than those for naphthalene. Anthracene is a reasonable surrogate for this study given its ubiquitous presence in combustion emissions[13−16] and its suspected toxicity.[17−22]

There are four previous studies of the reaction of OH with anthracene, all at low temperatures (58−470 K). The reported values express a large uncertainty in this reaction, ± a factor of 14. Biermann et al.[23] reported a rate constant for the reaction of anthracene with OH at 325 K of $110 \pm 9 \times 10^{-12}$ cm^3 molecule^{-1} s^{-1} using a relative-rate technique. Using the same approach, Kwok et al.[24−26] reported rate constants for the gas-phase reaction of anthracene with OH at room temperature and atmospheric pressure of air. Two separate studies resulted in rate coefficients of (13 ± 7) and $(17 \pm 6) \times 10^{-12}$ cm^3 molecule^{-1} s^{-1} at 296 and 297 K, respectively. Brubaker and Hites[27] reported rate constants for this reaction in a helium atmosphere using a miniature-scale, relative-rate technique. Rate coefficients of (183 ± 45) and $(180 \pm 46) \times 10^{-12}$ cm^3 molecule^{-1} s^{-1} were reported at 346 and 365 K, respectively. Most recently, Goulay et al.[28] reported the first absolute rate

* To whom correspondence should be addressed. E-mail: ananthula@udri.udayton.edu; taylor@udri.udayton.edu.

10.1021/jp054301c CCC: $33.50
Published on Web 02/15/2006

measurements of this reaction using a pulsed laser photolysis (PLP)/pulsed laser induced fluorescence (PLIF) technique over a temperature range of 58−470 K. The reported rate coefficients were 252, 127, 162, and 80 × 10^{-12} cm^3 $molecule^{-1}$ s^{-1} at 58, 119, 235, and 470 K, respectively. The authors reported an overall error of 30% for these rate coefficients, independent of temperature.

It is hypothesized[28,29] that two reaction pathways compete in the reaction of OH with aromatic rings. The first mechanism involves OH radical addition to the aromatic ring to form an energized OH−anthracene adduct $[C_{14}H_{10}-OH]^{\#}$, which is a reversible reaction. The energized adduct can either form a stabilized OH−anthracene adduct or form an alcohol via a H-displacement mechanism:

$$C_{14}H_{10} + OH \leftrightarrow [C_{14}H_{10}-OH]^{\#} \rightarrow C_{14}H_9OH + H$$
$$\downarrow$$
$$C_{14}H_{10}\text{-}OH$$

The second mechanism involves H atom abstraction by OH from anthracene leading to the formation of $C_{14}H_9$ and a water molecule:

$$C_{14}H_{10} + OH \rightarrow C_{14}H_9 + H_2O$$

The relative dominance of these pathways is dependent on temperature and pressure. This can be understood in the case of benzene,[9,28] where OH reactivity shows three distinct regimes as a function of temperature: (1) a slight positive temperature-dependent rate coefficient between 220 and 410 K, (2) a strong decrease in the rate constant between 410 and 525 K, and (3) a positive temperature-dependent rate coefficient above 525 K. This behavior is understood mechanistically as an OH-addition reaction below 410 K with dissociation of the OH-addition adduct back to reactants between 410 and 525 K. H abstraction is slow at low temperatures and becomes important only at temperatures greater than 500 K.

This manuscript reports the first extended temperature measurements for the reaction of OH with anthracene:

$$OH + \text{anthracene} \rightarrow \text{products} \quad k_1$$

$$OH + \text{anthracene-}d_{10} \rightarrow \text{products} \quad k_2$$

The available data on reaction of OH with anthracene are limited to low temperatures (<500 K) and are insufficient to ascertain the details of the reaction mechanism. There are no prior kinetic isotope measurements to distinguish between OH-addition and H-abstraction reaction channels. Furthermore, the available data do not provide any indication of the Arrhenius behavior of this reaction, especially at elevated temperatures.

The lack of both high-temperature measurements and a mechanistic understanding of the anthracene + OH reaction provide the primary motivation for this research. A secondary motivation for this study was to provide initial data for the assessment of the effect of molecular size on H-abstraction from aromatic species. These reactions are relevant in models of the molecular growth of soot precursors in flames.

Experimental Approach

The experimental procedures developed for pulsed laser photolysis/pulsed laser-induced fluorescence (PLP/PLIF) studies of the reaction of OH radicals with anthracene were based on recent studies of chlorinated hydrocarbons[30−32] and chlorinated dioxins.[33] The following paragraphs briefly summarize these procedures and discuss modifications to the experimental design to accommodate higher-temperature measurements with low-vapor pressure substrates.

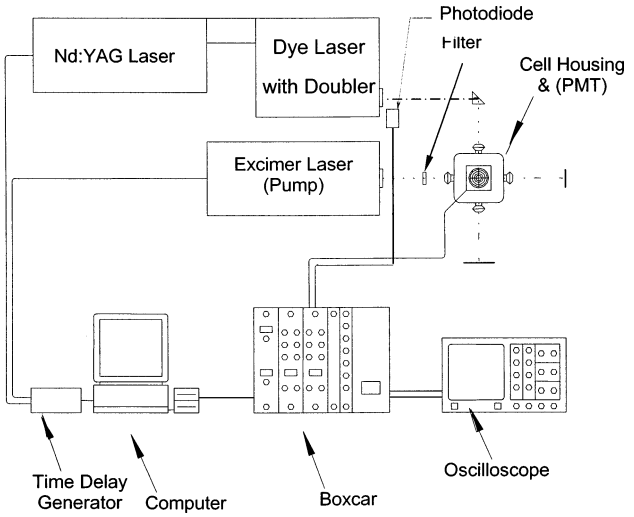

Figure 1. Schematic of PLP/PLIF apparatus.

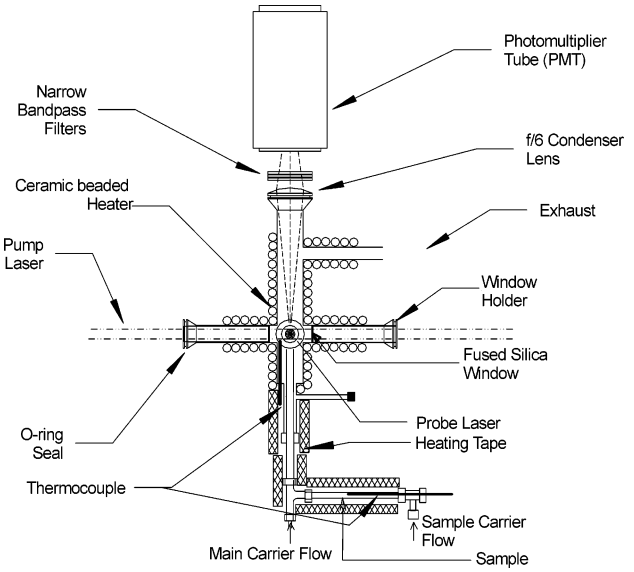

Figure 2. Schematic of optical reactor as modified for the anthracene + OH experiments.

Several improvements (Figures 1 and 2) have been made to the overall system to permit the acquisition of higher-precision rate coefficients for these low-vapor pressure compounds. An existing fused silica optical reactor was modified to achieve the following: (1) elimination of unheated recesses where substrate condensation can potentially occur, (2) incorporation of special grade fused silica windows to minimize leaks and provide optical stability for OH generation at temperatures in excess of 1000 K, and (3) minimization of the dead volume in the reactor by bringing the windows close to the reaction zone, thus reducing substrate condensation and the probability of multiple exposure of the substrate molecules to the photolysis laser during transit through the reactor. Experimental measurements were possible between ambient temperatures and 1200 K.

The second improvement to the system involved the incorporation of a higher-power pulsed Nd:YAG probe laser system (Continuum, Model 682-20/TDL-51, ∼5 mJ/cm^2/s @ 280 nm). This system permits OH measurements at absolute concentrations on the order of 10^{10} molecules cm^{-3}, a factor of ∼10 lower

TABLE 1: Experimental Parameters for Anthracene and Deuterated Anthracene Calibrations

anthracene			anthracene-d_{10}		
sample temperature (K)	sampling time (min)	sample flow rate (cm^3/min)	sample temperature (K)	sampling time (min)	sample flow rate (cm^3/min)
354	4	12	363	4	8
355	4	12	367	4	8
357	4	12	368	4	8
365	2	12	370	4	8
366	2	12	371	4	8
			372	4	8
			373	4	8

total flow in the reactor	100 cm^3/min
reactor temperature	250°C
sample trap	Tenax (GC 60/80 Mesh, Applied Science Laboratories Inc.)
GC-MS	Varian CP3800/Varian Saturn 2000 (Ion trap)
column	HP-5MS (Agilent Technologies), 30 m × 0.25 mm, 0.25 μ film thickness.

TABLE 2: Gas-Phase Concentration Data Derived from Reactor Sampling and GC-MS Quantitative Analysis for Anthracene and Anthracene-d_{10} (molar basis); Concentrations Are Also Shown from Recommended Temperature-Dependent Vapor Pressures for Anthracene

T (K)	gas-phase concentrated anthracene	anthracene concentrated (Hansen & Eckert[34])	T (K)	gas-phase concentrated anthracene-d_{10}
354	4.84×10^{-06}	5.55×10^{-06}	363	9.19×10^{-06}
357	6.67×10^{-06}	7.44×10^{-06}	367	1.68×10^{-05}
365	1.06×10^{-05}	1.59×10^{-05}	368	1.79×10^{-05}
366	1.18×10^{-05}	1.74×10^{-05}	370	1.75×10^{-05}
			371	2.39×10^{-05}
			372	2.53×10^{-05}
			373	2.63×10^{-05}

than our previous probe laser. The improved OH sensitivity permits exponential OH decays to be obtained at lower initial substrate concentrations, thus allowing measurements under more dilute conditions. This permits lower-temperature rate measurements for the less volatile PAH and also reduces errors due to secondary reactions. The third improvement involved the incorporation of a more versatile, pulsed Excimer pump laser (Lambda Physik, COMPEX 102). With this laser, pump laser energies can be easily varied, thus permitting a variety of OH radical precursors to be used. Nitrous oxide/water mixtures (193 nm) represent the cleanest overall source of OH radicals. This precursor combination can also be used to generate OH radicals over a fairly wide temperature range (up to ca. 1200 K).

Argon was used as a diluent and carrier gas for the OH precursors and substrate. PAH substrates were introduced with a heated sample inlet. The inlet consisted of a quartz tube that extends from the bottom of the reactor to the point of injection of the main carrier flow (see Figure 2). The substrate inlet contained milligram quantities of sample held in place with quartz wool. Recently published studies of OH reactions with chlorinated dioxins[33] verified that gas flows ranging from 1.5 to 10 cm^3/min were saturated with substrate vapor in the sample inlet using this design. Also, continuous measurement of the substrate temperature and carrier gas flow rate through the sample inlet permits sufficient control of the substrate concentration in the reactor.

Calibrations of the anthracene (and anthracene-d_{10}) concentration in the reactor as a function of inlet probe temperature provided an accurate estimate of the substrate concentration for each rate measurement. The experimental conditions for these calibrations are summarized in Table 1. Table 2 shows the gas-phase concentration of each substrate at different inlet probe temperatures before dilution with main carrier gas. Also presented in Table 2 are substrate-reactor concentrations derived from the temperature-dependent vapor pressure recommendation of Hansen and Eckert.[34] The substrate-reactor concentrations are reasonably consistent with the recommendations of Hansen and Eckert (within a factor of 0.5) and provide supporting evidence for saturation of the sample flow and quantitative transport of the substrate through the reactor.

A pulsed, 10 Hz, ArF excimer was used as the photodissociation source for N_2O/H_2O using Ar as the carrier gas. To a first approximation, secondary reactions were assumed to be negligible in their contribution to the measured rate because of the low initial OH concentrations and the single reaction, slow-flow reaction conditions. Thus, reactive fragments or molecules potentially produced by a variety of processes were swept out of the reaction volume before having an opportunity to react and cause a change in the measured rate.

Detection of OH radicals was achieved by PLIF, exciting the (1,0) band of the OH ($A^2\Sigma - X^2\Pi$) system at 282.2 nm. To reduce background signal level and increase discrimination of the OH fluorescence signal, three filters were used directly in front of the PMT. A dielectric composite band-pass filter (Acton Research Corporation: 308.5 nm, 11 nm FWHM), a Melles-Griot WG305 filter, and a Schott UG-11 filter together were employed to reduce undesired wavelengths. Time delays of 150−500 μs were employed to ensure that the OH radicals were thermalized during data collection.

Temperature-dependent kinetic data were collected from ca. 375 to 1200 K. To differentiate between OH-addition and H-abstraction reaction mechanisms, rate measurements on anthracene-d_{10} were performed at selected temperatures throughout the entire temperature range. All measurements were performed at 740 ± 10 Torr.

Data Reduction

Experiments were performed under pseudo-first-order kinetic conditions. Initial substrate concentrations ranged from 1 to 10 × 10^{12} molecules cm^{-3}, a large excess over calculated initial OH concentrations ((2−7) × 10^{10} molecules cm^{-3}). The OH concentrations were determined from the measured excimer laser fluence (2.25 mJ/cm^2, 193 nm), published values of the N_2O absorption coefficient[35] (8.95×10^{-20} cm^2/molecule at 298 K), a quantum yield of unity for singlet O atom production,[35] measured values of N_2O volumetric flow rate ((2.0−8.5) × 10^{14} molecules cm^{-3}), and rapid conversion of $O(^1D)$ atoms to OH radicals[32] (reaction stoichiometry of 2) by reaction with excess water vapor ((5.5−14.0) × 10^{15} molecules cm^{-3}). In the absence of photolytically and thermally generated secondary reactions, reactive and diffusive OH decay profiles were expected to

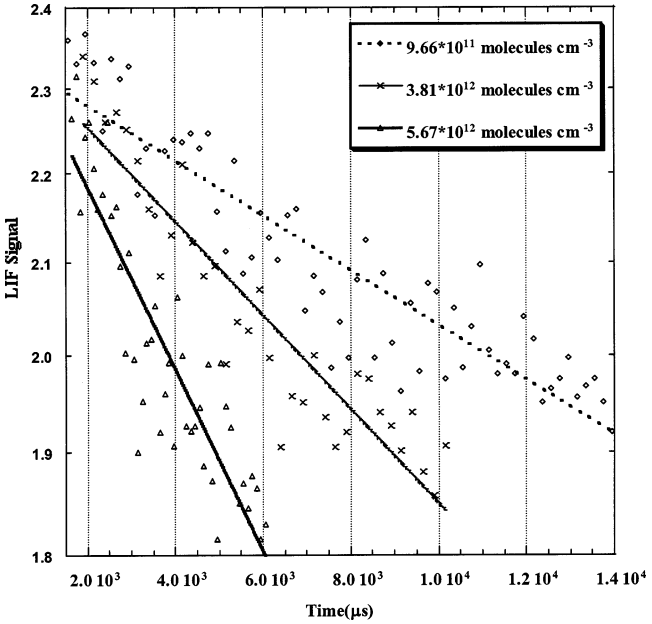

Figure 3. First-order decay of OH LIF signal with varying concentrations of anthracene at 399 K.

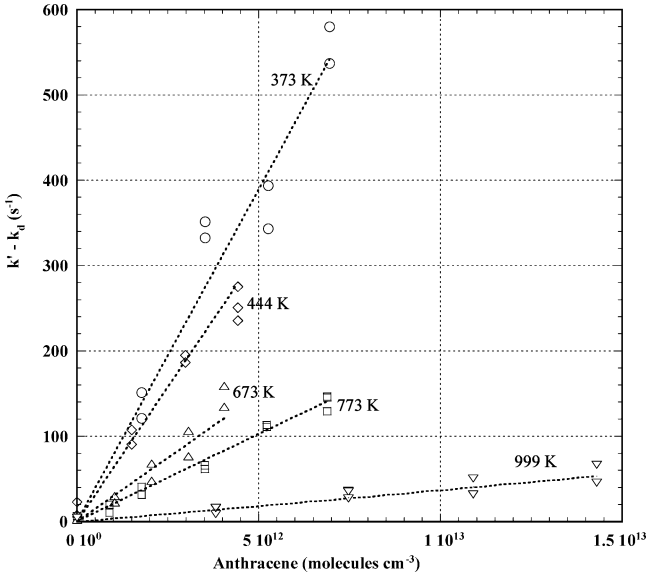

Figure 4. Plot of baseline-corrected pseudo-first-order rate coefficient, $k' - k_d$ (s^{-1}) versus anthracene concentration (molecules cm^{-3}) at selected reactor temperatures (symbols at each concentration represent multiple measurements).

exhibit exponential behavior and were fitted by the following nonlinear expression:

$$[OH] = [OH]_0 \exp(-k't) + \Gamma$$

where: [OH] = OH concentration at time t, $[OH]_0$ = initial OH concentration, k' = bimolecular rate constant, and Γ = background (constant) signal level from the probe laser. Because [OH] $\ll$ [substrate] in all reactive experiments, exponential "reaction only" [OH] dependences of pseudo-first-order decay constant $k' = k_{bi}$[substrate] were expected and observed. Figure 3 shows a typical exponential decay in the presence of varying concentrations of anthracene at 573 K. Figure 3 demonstrates that pseudo-first-order exponential OH decays were observed, confirming that the substrate concentration was in large excess of [OH]. Bimolecular rate coefficients, k_{bi}, were obtained from the slope of the least-squares straight line through the ([substrate], k') data points.

High purity anthracene and deuterated anthracene stock samples were purchased from commercial vendors (Aldrich, Inc. and Cambridge Isotope Labs, Inc.). Stated purities (99%) were verified by GC-MS analysis. Initial anthracene concentrations for a kinetic rate determination were typically varied by factors of 6−9, with lower and upper concentration limits of ca. 1×10^{12} molecules cm^{-3} and ca. 1×10^{13} molecules cm^{-3}, respectively. Figure 4 presents a plot of $k'-k_d$, pseudo-first-order rate constant versus substrate concentration at selected temperatures for anthracene.

Results

Room-temperature measurements were not possible due to the low vapor pressure of the substrate (0.0014 Pa[36] at 300.85 K). The lowest temperature where pseudo-first-order conditions could be achieved was 373 K.

Gas-phase ultraviolet absorption studies for anthracene at temperatures between 423 and 823 K indicate modest absorption below 200 nm (ca. $(1-2) \times 10^{-17}$ cm^2 $molecule^{-1}$).[12] Nonetheless, separate experiments were conducted to confirm that substrate photolysis was minimized at 193 nm. Anthracene flowing through the reactor was sampled and quantitative analyzed by GC-MS (see Table 1 for experimental conditions) with and without laser fluences of 15 mJ/cm^2/pulse. There was no evidence of loss of the substrate or the formation of substrate photolysis byproducts in the resulting chromatograms. The laser fluence employed for the bimolecular rate determinations was reduced by a factor of ca. 6 (2.25 mJ/cm^2/pulse) to further ensure that substrate photolysis did not impact the rate measurements.

TABLE 3: Rate Constants of Anthracene (k_1) and Anthracene-d_{10} (k_2)

T (K)	concentrated 10^{12} (molecule/cm^3)	$k_1 \pm 2\sigma$ 10^{-12} (cm^3/molecule-s)	T (K)	concentrated 10^{12} (molecule/cm^3)	$k_2 \pm 2\sigma$ 10^{-12} (cm^3/molecule-s)	KIE (k_1/k_2)
373	1.78−6.94	78.08 ± 8.97				
399	0.89−6.96	75.57[a] ± 7.75	398	2.20−8.58	59.22 ± 5.03	1.28
444	1.02−6.01	59.04[b] ± 5.05	423	1.63−6.36	74.71 ± 4.08	
498	0.70−5.59	55.63[a] ± 3.71	498	1.56−6.09	66.63 ± 2.12	0.83
573	0.39−4.75	35.20[a] ± 3.26	573	1.49−5.85	37.30 ± 2.92	0.94
673	0.76−5.92	29.62[a] ± 2.50	673	1.45−5.66	22.65 ± 1.49	1.31
773	0.40−6.88	14.70[a] ± 1.29	773	1.77−6.83	13.56 ± 1.48	1.08
923	0.71−5.49	5.65 ± 0.78				
999	3.82−14.27	3.72 ± 0.38	997	3.41−25.15	2.90 ± 0.15	1.28
1015	2.05−11.63	4.48 ± 0.47				
1053	1.96−14.53	3.94 ± 0.35				
1106	1.88−13.91	4.63 ± 0.29	1100	1.99−14.68	2.98 ± 0.22	1.55
1200	1.61−11.91	5.15 ± 0.40	1200	2.20−16.28	3.99 ± 0.57	1.29

[a] Average of three determinations. [b] Average of two determinations.

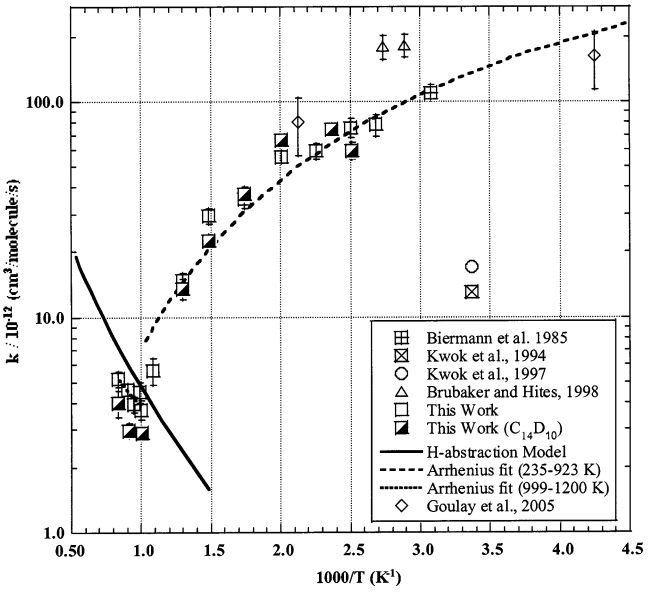

Figure 5. Arrhenius plot of k_1 and k_2. Error bars are $\pm 2\sigma$ limits. The dashed lines represent a modified Arrhenius fit to our measurements and the reported rate coefficient of Goulay et al.[28] at 235K. The solid line is a transition state theory calculation (see text). Also shown are previous measurements.[23−28]

Absolute rate measurements for k_1 (anthracene) and k_2 (anthracene-d_{10}) were carried out between 373 and 1200 K and are presented in Table 3. The 95% confidence intervals ($\pm 2\sigma$) ranged from 5 to 15%. The results along with previous measurements are presented in an Arrhenius plot in Figure 5. The rate coefficients near 470 K are in agreement, within experimental uncertainties, with the data of Goulay et al.[28] The data, when extrapolated to lower temperatures, is also in agreement with the Biermann et al.[23] reported rate coefficient at 325 K, a factor of 6 higher than the Kwok et al.[24−26] reported rate coefficients at 296 and 297 K, and a factor of 2 lower than Brubaker and Hites[27] reported rate coefficients at 346 and 365 K, respectively. The measurements reported by Kwok et al., however, were deduced based on anthracene impurities present in phenanthrene[24] and 1,2-dihydroanthracene,[25] and the authors themselves report their measurements as "approximate". The general agreement of the absolute and relative rate measurements at lower temperatures indicate that the order of magnitude of the rate constant is 10^{-10} cm^3 molecule^{-1} s^{-1} near room temperature, and that the approximate measurement of Kwok et al. is erroneously low.

The magnitude of the rate coefficients decreases slowly between 373 and 673 K and then much more rapidly (a factor of 9) from 673 to 923 K. The anthracene + OH rate measurements between 373 and 923 K were best fit by the following modified Arrhenius expression (in units of cm^3 molecule^{-1} s^{-1}):

$$k_1\,(373-923\ \mathrm{K}) = 8.17 \times 10^{14}\, T^{-8.3} \exp(-3171.71/T)$$

To extend the data set to atmospheric temperatures, the anthracene + OH rate measurements between 373 and 923 K and Goulay et al.'s reported rate coefficient at 235 K were combined and fit to the following modified Arrhenius expression (in units of cm^3 molecule^{-1} s^{-1}), represented by the dashed curve in Figure 5:

$$k_1\,(235-923\ \mathrm{K}) = 3136.70 \times T^{-4.7} \exp(-1108.18/T)$$

TABLE 4: Transition State Frequencies (cm^{-1}) and Rotational Constants (GHz)

H Abstraction from α Position			H Abstraction from β Position		
−1786	98	99	−1796	58	78
181	201[a]	232	177	196[a]	215
356	385	436	350	381	419
496	531	540	502	517	538
561	649	676	584	650	665
767	794	829	767	806	811
837	853	864	819	869	883
936	970	985	922	962	989
1037	1052	1075	1027	1041	1057
1093	1109	1142	1065	1099	1134
1203	1216	1227	1197	1213	1221
1273	1299	1335	1274	1308	1341
1411	1457	1483	1433	1435	1474
1498	1550	1575	1510	1547	1572
1636	1727	1759	1641	1738	1751
1799	3300	3303	1797	3300	3302
3312	3317	3322	3305	3311	3319
3330	3332	3993	3330	3331	4000
Rotational Constants			Rotational Constants		
1.517	1.111	0.644	2.757	0.694	0.557

[a] Vibrational frequencies correspond to $C_{10}H_7-HOH$ rotations that were treated as a hindered internal rotational contribution.

The anthracene + OH rate measurements between 1000 and 1200 K exhibited an apparent positive temperature dependence and were best fit by the following Arrhenius expression (in units of cm^3 molecule^{-1} s^{-1}), represented by the dashed curve in Figure 5:

$$k_1\,(999-1200\ \mathrm{K}) = 2.18 \times 10^{-11} \exp(-1734.11/T)$$

Discussion

The observed complex temperature-dependent behavior is consistent with previously published results for benzene and naphthalene.[9,29,37] To differentiate between OH-addition and H-abstraction reaction mechanisms, kinetic rate measurements were also performed on deuterated anthracene (see Table 3 and Figure 5). The rate coefficients obtained below 773 K for anthracene and deuterated anthracene were equal, within experimental error, and provide strong evidence that the reaction mechanism involves initial OH addition to the aromatic ring at temperatures below 1000 K.

Above 1000 K, although both k_1 and k_2 displayed a positive temperature dependence, there was no clear evidence of a KIE significantly greater than unity. Recent theoretical studies[29] for the benzene + OH H-abstraction reaction indicate the KIE is highly temperature dependent, with values ranging from ca. 4 at 500 K to ca. 1.7 at 1200 K. The lack of similar temperature dependence in our measurements is potentially due to the greater overlap of the two reaction mechanisms for anthracene, with an OH-addition-based mechanism dominant at temperatures below 1000 K and H abstraction growing in importance above 1000 K.

The positive KIE values are not large enough to be treated as convincing evidence for the H abstraction mechanism above 1000 K due to: (1) the relatively large uncertainty in these experimental determinations of the KIE (due to the separate measurements of k_H and k_D) and (2) the measured rate coefficient likely includes contributions from both OH addition and H abstraction. To provide further interpretation of the high-temperature measurements, the rate coefficient for H abstraction by OH was calculated using naphthalene as a surrogate compound. Density Functional Theory (DFT), KMLYP,[38] was

TABLE 5: Calculated Total Energies Using KMLYP/6-31G(d,p)

1 position	KMLYP/ 6-31G(d,p) (hartree)	zero-point correction (hartree)	thermal correction (hartree)	total energy at 0 K (hartree)	total energy at 298 K (hartree)	relative energy at 0 K (kcal/mol)	relative energy at 298 K (kcal/mol)
naphthalene	−385.12	0.154509	0.00932	−384.96	−384.96		
OH	−75.58	0.008985	0.003303	−75.57	−75.57		
TSα	−460.69	0.160475	0.009776	−460.53	−460.53	3.2	1.4
$C_{10}H_7(\alpha)$	−384.42	0.141135	0.007416	−384.28	−384.27	0.5[a]	−0.4[a]
H_2O	−76.28	0.022572	0.003779	−76.25	−76.25		
TSβ	−460.69	0.159995	0.009971	−460.53	−460.52	4.1	2.4
$C_{10}H_7(\beta)$	−384.42	0.140966	0.007419	−384.28	−384.27	0.1[b]	−0.8[b]

[a,b] Relative energy difference between reactants (naphthalene + OH) and products ($C_{10}H_7$ + H_2O).

TABLE 6: Thermodynamic Properties Used for TST Calculation

species	$H_{f,298}$[a]	S_{298}[b]	C_{P300}[b]	C_{P400}	C_{P500}	C_{P600}	C_{P800}	C_{P1000}	C_{P1500}
OH[c]	9.32	43.91	7.16	7.09	7.06	7.06	7.15	7.33	7.87
naphthalene[d]	36.0	80.57	32.01	43.3	52.75	60.32	71.33	78.82	89.86
H abstraction from α position (transition state)	46.7	95.17	37.19	48.6	58.29	66.09	77.42	85.15	96.51
H abstraction from β position (transition state)	47.8	97.4	37.53	48.67	58.18	65.89	77.2	84.96	96.38

[a] Unit in kcal/mol. [b] Unit in cal/mol-K. [c] Reference 43. [d] Reference 40−42.

applied to calculate thermodynamic properties of transition state (TS) compounds and products for the following reactions:

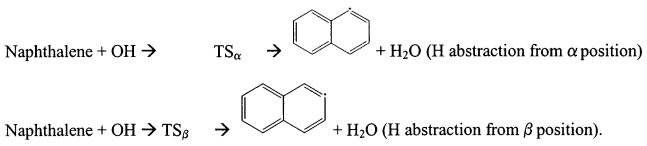

The geometry optimization and frequency calculation were performed using KMLYP/6-31G(d,p). Entropy ($S°_{298}$) and heat capacities ($C_P(T)$ $300 \le K \le 1500$) were calculated based on the moments of inertia and frequencies along with statistical mechanics. Contribution of hindered internal rotational mode for $S°_{298}$ and $C_P(T)$ were calculated separately based on the rotational barrier height and moments of inertia. Based on the vibrational mode analysis, the 5th lowest frequency corresponds to the naphthalene−HOH rotor. Single point calculation using KMLYP /6-31G(d,p) was applied to calculate the rotational barrier height. The general treatment of internal rotation of Pitzer et al.[39] was used to calculate hindered internal rotational contribution to $S°_{298}$ and $C_P(T)$. Two peaks (4.12 and 2.94 kcal/mol) were found for the naphthalene−HOH rotor at the α position, and the average value was used for the calculation. One peak (2.47 kcal/mol) was found for the naphthalene−HOH rotor at the β position. The thermodynamic properties of the reactants were taken from the literature.[40−42] The enthalpies of formation ($\Delta H_{f,298}$) of the TSs and products were calculated based on the $\Delta H_{f,298}$ of reactants obtained from literature and the energy difference between the reactants and corresponding compounds calculated at the KMLYP/6-31G(d,p) level of theory. The calculated frequencies, energies, and thermodynamic properties are shown in Tables 4, 5, and 6, respectively. For each reaction, the reaction rates were calculated using Transition State Theory (TST)[43] and fitted to the three-parameter Arrhenius expression, $k = A\,(T)^n \exp(-E_a/RT)$, over the temperature range of 500 to 2000 K. The calculated rate constants are shown in Table 7 and compared to previous naphthalene + OH measurements in Figure 6. Good agreement with rate measurements above 500 K was observed.

To apply the calculated rate of H abstraction from naphthalene to anthracene, the following assumptions were made: (1) H abstraction rates for all α positions of anthracene are identical, (2) H abstraction rates for α positions of anthracene are equal to those of α positions of naphthalene, (3) H abstraction rates for all β positions of anthracene are identical, and (4) H abstraction rates for β positions of anthracene are equal to those of β positions of naphthalene. Based on the geometric configuration of anthracene and naphthalene (see Figure 8), there are four β positions for both anthracene and naphthalene and six and four α positions for anthracene and naphthalene, respectively. The H-abstraction rate from anthracene can thus be calculated as:

TABLE 7: Calculated Rate Constants for H Abstraction from α and β Positions of Naphthalene

	reactions	A (cm^3/mol-s)	n	E_a (kcal/mol)
α	naphthalene + OH → $C_{10}H_7$ + H_2O	2.42×10^{-16}	1.38	1.67
β	naphthalene + OH → $C_{10}H_7$ + H_2O	1.36×10^{-15}	1.30	2.86

$$k_{ab} = k_\alpha \times 3/2 + k_\beta$$

where, k_α is the H-abstraction rate for all α positions of naphthalene together, and k_β is the H-abstraction rate for all β position of naphthalene together. The calculated rate was fit from 673 to 1873 K and resulted in the following expression:

$$k_{ab} = 9.57 \times 10^{-16}\, T^{1.39} \exp(-1106.14/T)$$

The calculated rate is plotted as a solid curve in Figure 5. The calculated rate overestimates the measured rate coefficients by a factor of 1.5.

A similar theoretical calculation was considered for OH addition to anthracene using naphthalene as a surrogate compound. However, comparison of OH reactivity with naphthalene[9,37] and anthracene (this study) shows a large difference at low temperature, as large as a factor of 8 at room temperature, as shown in Figure 8. This difference implies that the same assumption made for the theoretical calculation of H abstraction cannot be applied for OH addition. Goulay et al.[28] stated that the 9 and 10 positions of anthracene, which are represented by bold "α" sites in Figure 6, were more reactive with OH than the other carbon sites. They suggested that the carbon with the most positive net charge was the most reactive, and carbon 9 and 10 exhibit the largest positive net charge according to the semiempirical molecular orbital (MO) calculations conducted by Brubaker et al.,[27] and Biermann et al.[23] found that OH

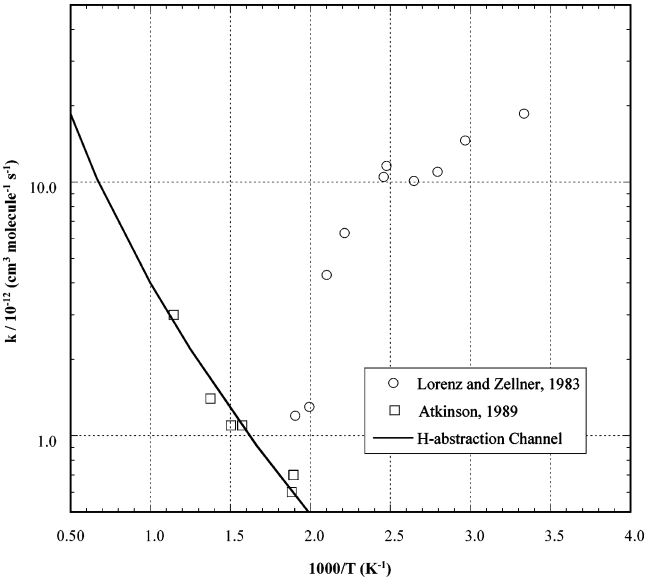

Figure 6. Arrhenius plot for the naphthalene + OH reaction. Shown are kinetic measurements from Lorenz and Zellner[37] ($T < 525$ K), unpublished results by Lorenz and Zellner ($T > 525$ K) presented in a compilation by Atkinson,[9] and the results of a transition state theory calculation (see text).

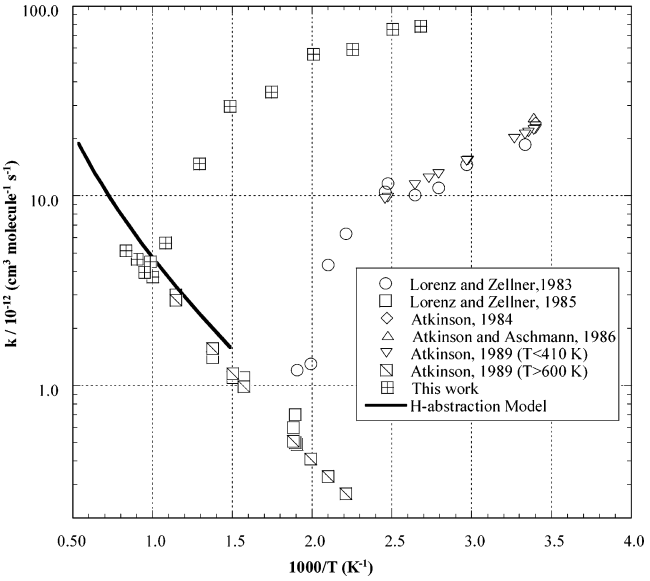

Figure 7. Arrhenius plot of our anthracene + OH measurements (denoted as "this work") in comparison with naphthalene + OH literature data.[9,37]

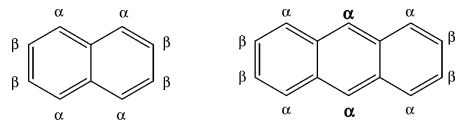

Figure 8. Molecular structure and sites of OH reaction for naphthalene (left) and anthracene (right).

reaction with phenanthrene was much smaller than OH reaction with anthracene, and this difference in reactivity was confirmed by MO calculations conducted by Klamt et al.[44]

We are currently conducting higher level DFT calculations for the OH-addition reaction to anthracene at 1, 2, and 9 positions to investigate this reactivity, with the results to be presented in a future paper.

To further investigate the relative importance of OH-addition and H-abstraction mechanisms in our rate measurements

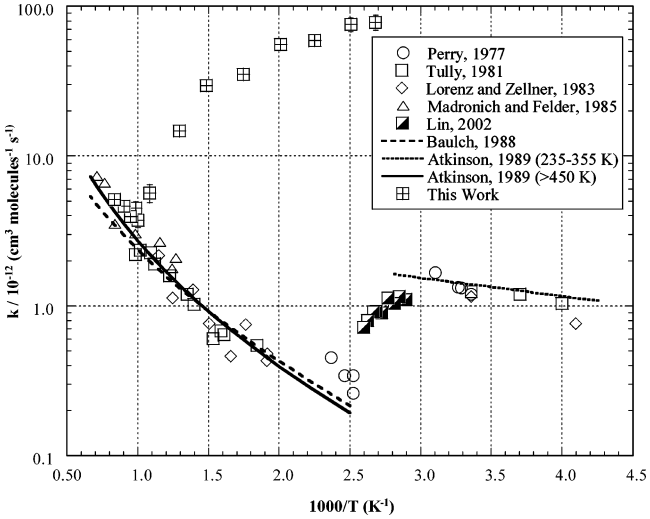

Figure 9. Arrhenius plot of our anthracene + OH measurements (denoted as "this work") in comparison with benzene + OH literature data.[9,29,37]

TABLE 8: Calculated KIE for H Abstraction from Anthracene

T (K)	(k_H/k_D)
800	4.14
1000	3.13
1200	2.61
1500	2.17
2000	1.82

between 1000 and 1200 K, the reaction rate of H abstraction via OH attack on deuterated anthracene was theoretically estimated using the same method applied for nondeuterated anthracene. The ratio of the respective rate constants (k_H/k_D) between 800 and 2000 K are shown in Table 8. Because no calculation was performed for OH addition to anthracene using naphthalene as a surrogate due to the reasons stated above, we were not able to calculate a true theoretical KIE value for this reaction. The true KIE will most likely be smaller than the values shown in Table 8, because no KIE is expected for the addition channel. However, until a comprehensive analysis of the OH addition and H abstraction at the 1, 2, and 9 positions of anthracene is performed, the relative importance of OH-addition and H-abstraction mechanisms at elevated temperatures cannot be elucidated. It also needs to be pointed out that the C−H bond dissociation from the anthracene−OH adduct at the OH-addition site is another source of KIE, and it will be included for the currently conducted theoretical calculations.

Conclusions and Implications for Atmospheric and Combustion Chemistry

The kinetics of the reaction of OH radicals with anthracene and deuterated anthracene were investigated between 375 and 1200 K using the PLP/PLIF technique. Extrapolation of the data to lower temperatures is generally consistent with previous absolute and relative rate measurements[23,27,28] (± a factor of 2), excluding the measurements of Kwok et al.[24−26] This suggests that the rate coefficient for anthracene + OH at 298 K is very fast, ca. 10^{-10} cm^3 molecule^{-1} s^{-1}.

The Arrhenius behavior of the measurements was very complex, suggesting the interplay of multiple reaction mechanisms. The low-temperature measurements (≤773 K) were consistent with an OH-addition mechanism. Theoretical analysis of KIE values above 1000 K indicates that H abstraction is a minor pathway with OH addition still dominant.

These OH measurements provide the first extended temperature data set for this important class of molecules. In comparison to benzene measurements at the high-pressure limit (see Figure 9), anthracene reactivity exhibits some important differences in the OH-addition regime relevant to combustion chemistry. The OH-addition mechanism appears to be dominant in anthracene for temperatures as high as 773 K as compared to 410 K for benzene, and the rate coefficient is larger by nearly 2 orders of magnitude at room temperature. The difference in rates of benzene compared to those of anthracene decreases with increasing temperatures with similar rates for anthracene and benzene in the H-abstraction regime above 1000 K. In comparison to naphthalene measurements at the high-pressure limit (see Figure 7), anthracene reactivity exhibits a similar trend. The OH-addition mechanism appears to be dominant in anthracene for temperatures as high as 773 K as compared to 525 K for naphthalene, and the rate coefficient is larger by nearly 1 order of magnitude at room temperature. The difference in rates for naphthalene and anthracene also decreases with increasing temperatures, with similar rates observed at ca. 1000 K. At higher temperatures (500−1000 K), the anthracene measurements do not exhibit evidence for a rapid change in mechanism from OH addition to H abstraction. In fact, there is no clear separation of these two mechanisms below 1000 K as is evident for benzene + OH and to a lesser extent, naphthalene + OH. Although the temperature where H abstraction is observed was shifted to higher temperatures for anthracene + OH (ca. 1000 K), the magnitude of the H-abstraction rate is not significantly different compared to benzene and naphthalene. To summarize, these initial results for a multiple ring PAH indicate that an increase in molecular size has a significant positive effect on the OH-addition rate, whereas the rate of H abstraction does not appear to change.

Acknowledgment. We gratefully acknowledge the National Science Foundation, Dr. Linda Blevins, Project Officer, for financial support of this research through assistance agreement CTS-0204759. R.A. also acknowledges the Dayton Area Graduate Studies Institute for financial support.

References and Notes

(1) Goldaniga, A.; Faravelli, T.; Ranzi, E. *Combust. Flame* **2000**, *122*, 350−358.
(2) Krestinin, A. V. *Combust. Flame* **2000**, *121*, 513−524.
(3) Richter, H.; Howard, J. B. *Prog. Energy Combust. Sci.* **2000**, *26*, 565−608.
(4) Scott, C. D. *J. Nanosci. Nanotechnol.* **2004**, *4*, 368−376.
(5) Lahaye, J., Prado, G., Eds.; *Soot in Combustion Systems and Its Toxic Properties*; Plenum Press: New York, 1981.
(6) Siegla, D. C., Smith, G. W., Eds.; *Particulate Carbon Formation During Combustion*; Plenum Press: New York, 1981.
(7) Jander, H., Wagner, H. G., Eds.; *Soot Formation in Combustion*; Vandenhoeck & Ruprecht: Göttingen, Germany, 1990.
(8) Bockhorn, H., Ed.; *Soot Formation in Combustion: Mechanisms and Models*, Springer: Berlin, 1994.
(9) Atkinson, R. *J. Phys. Chem. Ref. Data*, Monograph, **1989**, 1.
(10) Saunders, S. M.; Jenkin, M. E.; Derwent, R. G.; Pilling, M. J. *Atmos. Environ.* **1997**, *31*, 1249−1250.
(11) Fan, Z.; Chen, D.; Birla, P.; Kames, R. M. *Atmos. Environ.* **1997**, *31*, 1249−1250.
(12) Andreas, T.; Michel, J. R. *J. Photochem. Photobio. A: Chem.* **1997**, *104*, 25−23.
(13) Narsin, R. K.; Peter, A. S.; Thomas, M. H. *Atmos. Environ.* **1995**, *29*, 533−542.
(14) Tavares, M., Jr.; Pinto, J. P.; Souza, A. L.; Scarmínio, I. S.; Solci, M. C. *Atmos. Environ.* **2004**, *38*, 5039−5044.
(15) Lee, W. J.; Wang, Y. F.; Lin, T. C.; Chen, Y. Y.; Lin, W. C.; Ku, C. C.; Cheng, J. T. *Sci. Total Environ.* **1995**, *159*, 185−200.
(16) Zimmermann, R.; Heger, H. J.; Kettrup, A.; Boesl, U. *Rapid Commun. Mass Spectrom.* **1997**, *11*, 1095−1102.
(17) Tsai, P. J.; Shieh, H. Y.; Lee, W. J.; Lai, S. O. *J. Hazard. Mater. A* **2002**, *91*, 25−42.
(18) Thomas, P.; Peter, S.; Christian, S. *Chemosphere* **1996**, *32*, 639−648.
(19) U. S. EPA. Health and Environmental Effects Profile for Anthracene. http://www.epa.gov/iris/subst/0434.htm. Prepared by the Office of Health and Environmental Assessment, Environmental Criteria and Assessment Office, Cincinnati, OH, for the Office of Solid Waste and Emergency Response, Washington, DC, 1987.
(20) Agency for Toxic Substances and Disease Registry (ATSDR). http://www.atsdr.cdc.gov/toxprofiles/tp69.html. (PB/95/264370), Aug 1995.
(21) Falkson, G.; Klein, B.; Falkson, H. *Exp. Hematol.* **1985**, *13*, 64−71.
(22) Volkova, N. I. In *Encyclopedia of Occupational Health and Safety*; Parmeggiani, L., Ed.; International Labour Office: Geneva, 1983; Vol. 1, 162−163.
(23) Biermann, H. W.; MacLeod, H.; Atkinson, R.; Winer, A. M.; Pitts, J. N., Jr. *Environ. Sci. Technol.* **1985**, *19*, 244−248.
(24) Kwok, E. S. C.; Harger, W. P.; Arey, J.; Atkinson, R. *Environ. Sci. Technol.* **1994**, *28*, 521−527.
(25) Kwok, E. S. C.; Atkinson, R.; Arey, J. *Int. J. Chem. Kinet.* **1997**, *29*, 299−309.
(26) Kwok, E. S. C.; Atkinson, R. *Atmos. Environ.* **1995**, *29*, 1685−1695.
(27) Brubaker, W. W.; Hites, R. A. *J. Phys. Chem. A.* **1998**, *102*, 915−921.
(28) Goulay, F.; Rebrion-Rowe, C.; Le Garrec, J. L.; Le Picard, S. D.; Canosa, A.; Rowe, B. R. *J. Chem. Phys.* **2005**, *122*, 104308.
(29) Tokmakov, I. V.; Lin, M. C. *J. Phys. Chem. A* **2002**, *106*, 11309−11326.
(30) Tichenor, L. B.; Graham, J. L.; Yamada, T.; Taylor, P. H.; Peng, J.; Hu, X.; Marshall, P. *J. Phys. Chem. A* **2000**, *104*, 1700−1707.
(31) Yamada, T.; El-Sinawi, A.; Siraj, M.; Taylor, P. H.; Peng, J.; Hu, X.; Marshall, P. *J. Phys. Chem. A* **2001**, *105*, 7588−7597.
(32) Yamada, T.; Siraj, M.; Taylor, P. H.; Peng, J.; Hu, X.; Marshall, P. *J. Phys. Chem. A* **2001**, *105*, 9436−9444.
(33) Taylor, P. H.; Yamada, T.; Neuforth, A. J. *Chemosphere* **2005**, *58*, 243−252.
(34) Hansen, P. C.; Eckert, C. A. *J. Chem. Eng. Data* **1986**, *31*, 1−3.
(35) DeMore, W. B.; Sander, S. P.; Golden, D. M.; Hampson, R. F.; Kurylo, M. J.; Howard, C. J.; Ravishankara, A. R.; Kolb, C. E.; Molina, M. J. *Chemical Kinetics and Photochemical Data for Use in Stratospheric Modeling*, Evaluation Number 12; Jet Propulsion Laboratory, Publication 97-4, 1997.
(36) Oja, V.; Suuberg, E. M. *J. Chem. Eng. Data* **1998**, *43*, 486-492.
(37) Lorenz, K.; Zellner, R. *Ber. Bunsen-Ges. Phys. Chem.* **1983**, *87*, 629−636.
(38) Kang, J. K.; Musgrave, Ch. B. *J. Chem. Phys.* **2001**, *115*, 11040−11051.
(39) Pitzer, K. S.; Gwinn, W. *J. Chem. Phys.* **1942**, *10*, 428−436.
(40) Coleman, D. J.; Pilcher, G. *Trans. Faraday Soc.* **1966**, *62*, 821−827.
(41) *Selected Values of Properties of Chemical Compounds*; Texas A&M University: College Station, TX, 1997.
(42) Chase, M. W., Jr. *NIST-JANAF Thermochemical Tables*, 4th ed.; J. Phys. Chem. Ref. Data Monograph No. 9; National Institute of Standards and Technology: Gaithersburg, MD, 1998.
(43) Benson, S. W. *Thermochemical Kinetics*; Wiley-Interscience: New York, 1976.
(44) Klamt, A. *Chemosphere* **1994**, 26, 1273.